Engineering with Computers (2021) 37:3551–3567
https://doi.org/10.1007/s00366-020-01015-w

ORIGINAL ARTICLE

Development of a shell superelement for large deformation and free vibration analysis of composite spherical shells

Mansoor Shamloofard[1] · Ali Hosseinzadeh[2] · M. R. Movahhedy[1]

Received: 28 November 2019 / Accepted: 17 March 2020 / Published online: 12 April 2020

Abstract
Finite element analysis of huge and/or complicated structures often requires long times and large computational expenses. Superelements are huge elements that exploit the deformation theory of a specific problem to provide the capability of discretizing the problem with minimum number of elements. They are employed to reduce the computational cost while retaining the accuracy of results in FEM analysis of engineering problems. In this research, a new shell superelement is presented to study linear/nonlinear static and free vibration analysis of spherical structures with partial or full spherical geometries that exist in many industrial applications. Furthermore, this study investigates the effects of changing the superelement size and its number of nodes on solution accuracy. The governing equations of composite spherical shells are derived based on the first-order shear deformation theory and considering large deformations. For solving the nonlinear governing equations, the tangent stiffness matrix has been extracted and the Newton–Raphson method is employed. The capability of the presented shell superelement is investigated in several problems under linear/nonlinear static and free vibration analysis. The results acquired by the presented shell superelements are compared with available results in the literature and conventional shell elements in a commercial software. Results comparisons reveal high accuracy at a reduced computational cost in the superelement model.

Keywords Finite element analysis · Shell superelement · First-order shear deformation theory · Large deformation · Numerical analysis of composite spherical shell · Free vibration analysis

1 Introduction

Finite element method (FEM) has been widely used for analysis of engineering problems [1]. However, in some cases that the structure is huge or complicated, FEM requires tremendous computational costs [2]. This is mainly due to a large number of elements and nodes that should be considered for approximating the field variables in these problems. Recently, researchers have presented several approaches to overcome this shortcoming. In one approach, isogeometric analysis has been presented to eliminate the mesh generation process, which results in decreasing the solution time of engineering problems [3–5]. Another approach investigated in this study is the use of superelement, which considerably reduces the number of necessary elements and nodes, while providing an acceptable accuracy in the solution. Koko et al. [6, 7] analyzed stiffened plates using superelements. They used shear deformation theory and concluded that using superelements in nonlinear dynamic analysis of plates is highly efficient. Furthermore, they studied the vibration analysis of stiffened plates using their proposed superelement in Ref. [8]. Jiang et al. [9] studied static and dynamic analysis of stiffened cylindrical shells using superelements with considering geometric and material nonlinearities. Ahmadian et al. [10] investigated the free vibration analysis of composite plates using superelements.

In recent years, cylindrical, conical and spherical superelements have been introduced for static and vibration analysis of such structures. For instance, Bonakdar et al. [11] proposed a cylindrical superelement for static and

✉ M. R. Movahhedy
Movahhed@sharif.edu

[1] Department of Mechanical Engineering,, Sharif University of Technology, Azadi Avenue, P.O. Box 11365-9567, Tehran, Iran

[2] Isfahan University of Technology, Isfahan, Iran

dynamic analysis of multilayer composite cylinders. Also, Rezaei et al. [12] developed a tapered superelement to simulate tapered parts in the machine tools spindle. Furthermore, free vibration analysis of several FGM structures was studied by Torabi et al. [13] using a presented 3D superelement. The spherical superelement was initially presented by Nasiri et al. [14]. They studied static and free vibration analysis of the spherical structures using the presented superelement. Then, Shamloofard et al. [15] modified the spherical superelement designed in [14] and developed a thermo-elastic model of spherical and tapered superelements.

Laminated composite shells are frequently used in many structures, due to the high strength/weight ratio of composite structures [16, 17]. These structures are usually thin and are exposed to various and severe static and dynamic loads. Therefore, vibration behavior and deformation analysis of these structures are significantly important, and these issues have been recently discussed in many research studies. For instance, vibration characteristics of laminated doubly curved and spherical shells have been investigated by using different methods in Refs. [18–29]. In addition, deformation analysis of these shells has been studied by considering different approaches in Refs. [30–39].

The objective of this research study is to present a new shell superelement which is capable of discretizing complete and partial spherical shells and predicting linear/nonlinear static and free vibration behavior of composite spherical shells under local loads and boundary conditions. Moreover, this study recommends the optimum number of nodes in each shell superelement to achieve the best compromise between accuracy and computational cost. To the best of the authors' knowledge, this subject has not been investigated for spherical, conical and cylindrical superelements which have been presented in the literature.

In what follows, the finite element equations for spherical shells are initially derived using first-order shear deformation theory (FSDT), next a spherical shell superelement is presented, and finally, through several problems, the results obtained from the proposed superelement are compared with the existing results in the literature and conventional shell elements in ANSYS software.

2 Background theory and governing equations

Based on FSDT and considering the spherical coordinate system, a displacement field (U_ϕ, U_θ, W) is related to displacements and rotations of mid-plane of the plate through the following equation [40]:

$$\begin{aligned} U_\phi(\phi,\theta,\xi) &= u_\phi(\phi,\theta) + \xi\beta_\phi(\phi,\theta) \\ U_\theta(\phi,\theta,\xi) &= u_\theta(\phi,\theta) + \xi\beta_\theta(\phi,\theta) \\ W(\phi,\theta,\xi) &= w(\phi,\theta) \end{aligned} \tag{1}$$

where u_ϕ, u_θ and w are the displacement components for points lying on the middle surface of the shell along with meridional, circumferential and normal directions, respectively. Also, β_ϕ, β_θ and ξ are normal-to-mid-surface rotations and distance from the mid-surface, respectively. Strain–displacement relations used in this paper are formulated based on the extension of the Sanders theory [41] and deal with the large deformation in the von Karman sense stated in Ref. [42]. For this case of geometric nonlinearity, small strains and moderate rotations are taken into consideration [40]. Using these assumptions as well as the FSDT for spherical shells with a radius of R, the strain–displacement equations are deduced as follows:

$$\begin{Bmatrix} \varepsilon_\varphi \\ \varepsilon_\theta \\ \varepsilon_{\varphi\xi} \\ \varepsilon_{\theta\xi} \\ \varepsilon_{\varphi\theta} \end{Bmatrix} = \begin{Bmatrix} \varepsilon^0_\varphi \\ \varepsilon^0_\theta \\ \varepsilon^0_{\varphi\xi} \\ \varepsilon^0_{\theta\xi} \\ \varepsilon^0_{\varphi\theta} \end{Bmatrix} + \xi \begin{Bmatrix} \kappa_\varphi \\ \kappa_\theta \\ 0 \\ 0 \\ \kappa_{\varphi\theta} \end{Bmatrix}$$

$$\varepsilon^0_\varphi = \frac{1}{R}\left(\frac{\partial u_\varphi}{\partial\varphi} + w\right) + \frac{1}{2}\left(\frac{1}{R}\frac{\partial w}{\partial\varphi}\right)^2$$

$$\varepsilon^0_\theta = \frac{1}{R\sin(\varphi)}\frac{\partial u_\theta}{\partial\theta} + \frac{\cot(\varphi)}{R}u_\varphi + \frac{w}{R} + \frac{1}{2}\left(\frac{1}{R\sin(\varphi)}\frac{\partial w}{\partial\theta}\right)^2$$

$$\varepsilon^0_{\varphi\xi} = \frac{1}{R}\left(\frac{\partial w}{\partial\varphi} - u_\varphi\right) + \beta_\varphi$$

$$\varepsilon^0_{\theta\xi} = \frac{1}{R\sin(\varphi)}\frac{\partial w}{\partial\xi_2} - \frac{u_\theta}{R} + \beta_\theta$$

$$\varepsilon^0_{\varphi\theta} = \frac{1}{R}\frac{\partial u_\theta}{\partial\varphi} + \frac{1}{R\sin(\varphi)}\frac{\partial u_\varphi}{\partial\theta} - \frac{\cot(\varphi)}{R}v_0 + \left(\frac{1}{R}\frac{\partial w}{\partial\varphi}\right)\left(\frac{1}{R\sin(\varphi)}\frac{\partial w}{\partial\theta}\right)$$

$$\kappa_\varphi = \frac{1}{R}\frac{\partial\beta_\varphi}{\partial\varphi}$$

$$\kappa_\theta = \frac{1}{R\sin(\varphi)}\left(\frac{\partial\beta_\theta}{\partial\theta} + \frac{\cot(\varphi)}{R}\beta_\varphi\right)$$

$$\kappa_{\varphi\theta} = \frac{1}{R}\frac{\partial\beta_\theta}{\partial\varphi} + \frac{1}{R\sin(\varphi)}\frac{\partial\beta_\varphi}{\partial\theta} - \frac{\cot(\varphi)}{R}\beta_\theta \tag{2}$$

where the strains ε^0_φ, ε^0_θ and $\varepsilon^0_{\varphi\theta}$ are the in-plane meridional, circumferential and shearing components, $\varepsilon^0_{\varphi\xi}$ and $\varepsilon^0_{\theta\xi}$ are the transverse shearing strains, and κ_φ, κ_θ and $\kappa_{\varphi\theta}$ are the analogous curvature changes in the middle surface.

The relationship between stress resultants and couples with generalized strains and curvature variations on the middle surface can be summarized as:

$$\begin{aligned}\{Q^s\} &= [A^s]\{\beta\}\\ \{N\} &= [A]\{\varepsilon^0\} + [B]\{\kappa\}\\ \{M\} &= [B]\{\varepsilon^0\} + [D]\{\kappa\}.\end{aligned} \tag{3}$$

The strain vector $\{\varepsilon^0\}$ is expressed as the sum of the two linear and nonlinear strain vectors:

$$\{\varepsilon^0\} = \{\varepsilon^0\}_L + \{\varepsilon^0\}_{NL}. \tag{4}$$

Substituting Eq. (4) in Eq. (3) gives:

$$\begin{aligned}\{N\} &= [A]\{\varepsilon^0\}_L + [A]\{\varepsilon^0\}_{NL} + [B]\{\kappa\}, \{M\}\\ &= [B]\{\varepsilon^0\}_L + [B]\{\varepsilon^0\}_{NL} + [D]\{\kappa\}\end{aligned} \tag{5}$$

where the components of the extensional stiffness A, bending extensional coupling stiffness B, bending stiffness D and transverse shear stiffness A^s are defined as follows:

$$\begin{aligned}&\left(A_{ij}(\varphi,\theta), B_{ij}(\varphi,\theta), D_{ij}(\varphi,\theta)\right)\\ &\quad = \int_{-\frac{h}{2}}^{\frac{h}{2}} \bar{Q}_{ij}(\varphi,\theta)\left(1,\xi,\xi^2\right)\mathrm{d}\xi \quad i,j = 1,2,6\\ &A^s_{ij}(\varphi,\theta) = K^s \int_{-\frac{h}{2}}^{\frac{h}{2}} \bar{Q}_{ij}(\varphi,\theta)\mathrm{d}\xi \quad i,j = 4,5\end{aligned} \tag{6}$$

where h is the shell thickness and K^s is the shear correction factor, which is usually set to 5/6 [43]. Also, $\bar{Q}_{ij}$ represents the transformed reduced stiffness which is computed for any arbitrary kth layer as follows:

$$\begin{aligned}\bar{Q}^{(k)}_{11} &= Q^{(k)}_{11}m^4 + 2\left(Q^{(k)}_{12} + 2Q^{(k)}_{66}\right)n^2m^2 + Q^{(k)}_{22}n^4\\ \bar{Q}^{(k)}_{12} &= \left(Q^{(k)}_{11} + Q^{(k)}_{22} - 4Q^{(k)}_{66}\right)n^2m^2 + Q^{(k)}_{12}\left(n^4 + m^4\right)\\ \bar{Q}^{(k)}_{22} &= Q^{(k)}_{11}n^4 + 2\left(Q^{(k)}_{12} + 2Q^{(k)}_{66}\right)n^2m^2 + Q^{(k)}_{22}m^4\\ \bar{Q}^{(k)}_{66} &= \left(Q^{(k)}_{11} + Q^{(k)}_{22} - 2Q^{(k)}_{12} - 2Q^{(k)}_{66}\right)n^2m^2 + Q^{(k)}_{66}\left(n^4 + m^4\right)\\ \bar{Q}^{(k)}_{16} &= \left(Q^{(k)}_{11} - Q^{(k)}_{12} - 2Q^{(k)}_{66}\right)nm^3 + \left(Q^{(k)}_{12} - Q^{(k)}_{22} + 2Q^{(k)}_{66}\right)mn^3\\ \bar{Q}^{(k)}_{26} &= \left(Q^{(k)}_{11} - Q^{(k)}_{12} - 2Q^{(k)}_{66}\right)mn^3 + \left(Q^{(k)}_{12} - Q^{(k)}_{22} + 2Q^{(k)}_{66}\right)nm^3\\ \bar{Q}^{(k)}_{44} &= Q^{(k)}_{44}m^2 + Q^{(k)}_{55}n^2\\ \bar{Q}^{(k)}_{55} &= Q^{(k)}_{55}m^2 + Q^{(k)}_{44}n^2\\ \bar{Q}^{(k)}_{45} &= \left(Q^{(k)}_{44} - Q^{(k)}_{55}\right)nm\\ m &= \cos(\alpha_1); \quad n = \sin(\alpha_1)\end{aligned} \tag{7}$$

where α_1 is the fiber orientation angle of the k[th] lamina with respect to the shell coordinate system and elastic constants $Q^{(k)}_{ij}$ in each layer are given as follows:

$$\begin{aligned}&Q^{(k)}_{11} = \frac{E^{(k)}_1}{1 - v^{(k)}_{12}v^{(k)}_{21}}, \quad Q^{(k)}_{22} = \frac{E^{(k)}_2}{1 - v^{(k)}_{12}v^{(k)}_{21}}, \quad Q^{(k)}_{12} = \frac{v^{(k)}_{12}E^{(k)}_2}{1 - v^{(k)}_{12}v^{(k)}_{21}}\\ &Q^{(k)}_{66} = G^{(k)}_{12}, \quad Q^{(k)}_{44} = G^{(k)}_{13}, \quad Q^{(k)}_{55} = G^{(k)}_{23}\end{aligned} \tag{8}$$

where $E^{(k)}_1, E^{(k)}_2, G^{(k)}_{12}, G^{(k)}_{13}, G^{(k)}_{23}, v^{(k)}_{12}$ and $v^{(k)}_{21}$ are engineering parameters of the kth layer.

3 Finite element analysis

Based on FSDT, five degrees of freedom u_0, v_0, w_0, β_φ and β_θ are considered for each node of the superelement. Displacements and rotations of an arbitrary point (L) are calculated as follows:

$$\begin{aligned}u^L(\varphi,\theta) &= \sum_{i=1}^{npe} N_i(\varphi,\theta)u_i\\ v^L(\varphi,\theta) &= \sum_{i=1}^{npe} N_i(\varphi,\theta)v_i\\ w^L(\varphi,\theta) &= \sum_{i=1}^{npe} N_i(\varphi,\theta)w_i\\ \beta^L_\varphi(\varphi,\theta) &= \sum_{i=1}^{npe} N_i(\varphi,\theta)\beta_{\varphi i}\\ \beta^L_\theta(\varphi,\theta) &= \sum_{i=1}^{npe} N_i(\varphi,\theta)\beta_{\theta i}\end{aligned} \tag{9}$$

where u_i, v_i, w_i, $\beta_{\theta i}$ and $\beta_{\varphi i}$ are displacements and rotations of the node i, N_i is the shape function of node i, and npe is the number of nodes in each superelement. Equation (9) can also be described as the following equation:

$$\{u\}_{5\times1} = [N]_{5\times5npe}\{U\}_{5npe\times1}$$

$$[N] = \begin{bmatrix} N_1 & 0 & 0 & 0 & 0 & \dots & N_{npe} & 0 & 0 & 0 & 0\\ 0 & N_1 & 0 & 0 & 0 & \dots & 0 & N_{npe} & 0 & 0 & 0\\ 0 & 0 & N_1 & 0 & 0 & \dots & 0 & 0 & N_{npe} & 0 & 0\\ 0 & 0 & 0 & N_1 & 0 & \dots & 0 & 0 & 0 & N_{npe} & 0\\ 0 & 0 & 0 & 0 & N_1 & \dots & 0 & 0 & 0 & 0 & N_{npe} \end{bmatrix}_{5\times5npe} \tag{10}$$

where $\{U\}$ is the nodal displacement vector. Using Eq. (10), the relationship between nodal displacement vector with strain and curvature variations vectors can be deduced as below:

$$\begin{aligned}\{\varepsilon^0\}_L &= [L_m][N]\{U\} = [B_m]\{U\}\\ \{\kappa\} &= [L_b][N]\{U\} = [B_b]\{U\}\\ \{\beta\} &= [L_s][N]\{U\} = [B_s]\\ \{\varepsilon^0_{NL}\} &= [L_{NL}][N]\{U\} = [B_{NL}]\{U\}\end{aligned} \tag{11}$$

where $[B_m], [B_b], [B_s]$ and $[B_{NL}]$ are given in Appendix 1.

Following the finite element approach, the governing equation is concluded as follows:

$$KU = F$$
$$F = \sum_{i=1}^{ne} f_i^{(e)}, K = \sum_{i=1}^{ne} K_i^{(e)}$$
$$f^{(e)} = \iint_s [N]^T \{f_s\} \mathrm{d}A + \sum [N]^T \{f_c\} \tag{12}$$

where ne, F, f_s, f_c and K are the number of superelements, total force vector, traction force, concentrated force and stiffness matrix computed as follows:

$$K^{(e)} = K_1 + K_2 + K_3 + K_4 + K_5 + K_6 + K_7 + K_8 + K_9 + K_{10} \tag{13}$$

where $K_1, K_2, K_3, \ldots, K_{10}$ are presented in Appendix 2.

The solution algorithm for solving the governing equations (Eq. (12)) is the iterative method of Newton–Raphson described in Appendix 3.

3.1 Free vibration analysis

For free vibration analysis, natural frequencies (ω) are calculated according to the eigenvalue equation in which M is the mass matrix as follows:

$$\left(K - \omega^2 M\right)\lambda = 0$$
$$M^{(e)} = \iint_{A^e} [N]^T [\rho][N] \mathrm{d}A$$
$$[\rho] = \begin{bmatrix} \rho_0 & 0 & 0 & \rho_1 & 0 \\ 0 & \rho_0 & 0 & 0 & 0 \\ 0 & 0 & \rho_0 & 0 & 0 \\ \rho_1 & 0 & 0 & \rho_2 & 0 \\ 0 & 0 & 0 & 0 & \rho_2 \end{bmatrix} \tag{14}$$

where ρ_0, ρ_1 and ρ_2 are the normal, coupled normal-rotary and rotary inertial coefficients defined by:

$$(\rho_0, \rho_1, \rho_2) = \int_{-\frac{h}{2}}^{\frac{h}{2}} \rho(\xi)\left(1, \xi, \xi^2\right) \mathrm{d}\xi. \tag{15}$$

4 Spherical shell superelement

The purpose of introducing this superelement is to present an element that can easily discretize spherical sectors with and without apex and complete spherical shells with fewer elements. Polynomial and circular shape functions are employed to obtain this spherical shell superelement in meridional and circumferential directions, respectively. Figures 1 and 2 show the arrangement of nodes in these directions.

Along φ, Lagrange shape functions (polynomials) are utilized for approximating the field variables. By setting M nodes in this direction, shape functions have the following form:

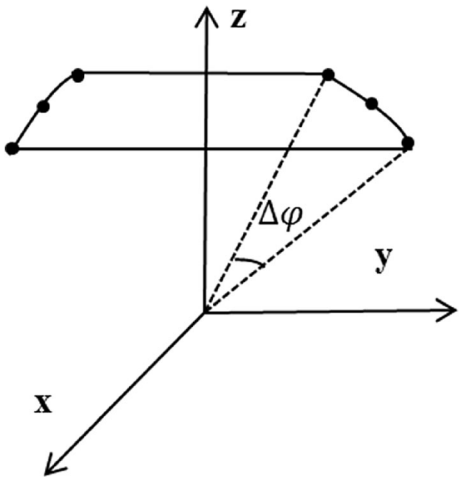

Fig. 1 Arrangement of nodes in the meridional direction where three nodes are used in this direction

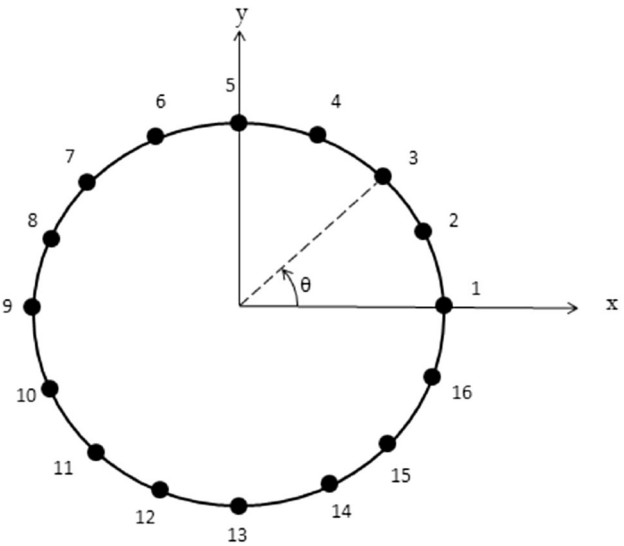

Fig. 2 Arrangement of nodes in the circumferential direction where 16 nodes are used in this direction

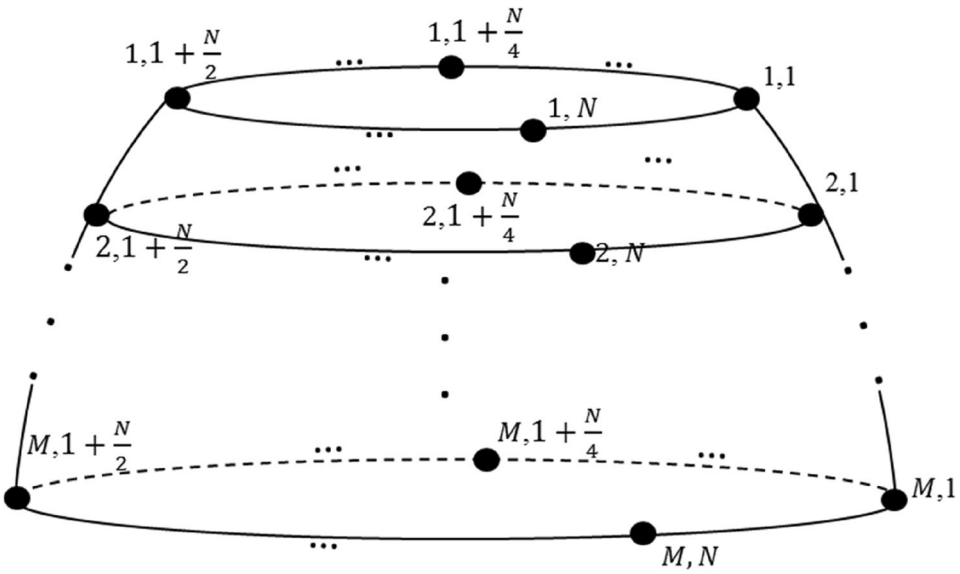

Fig. 3 $(M \times N)$-node superelement without a pole

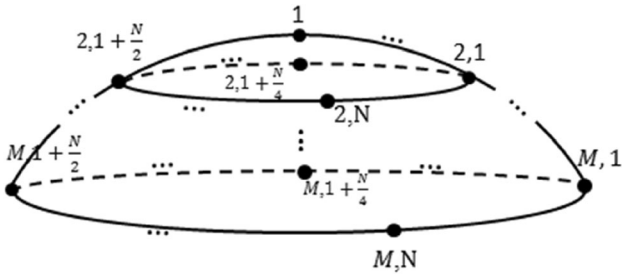

Fig. 4 $(1 + N * (M - 1))$-node superelement including pole

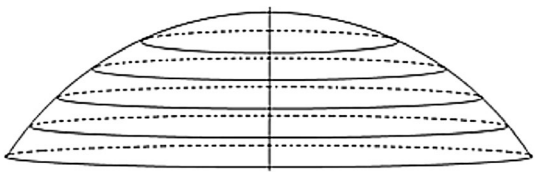

Fig. 5 Increasing the number of superelements

$$N_i^{(\varphi)} = A_1 + A_2\varphi + \cdots + A_M\varphi^{M-1} \quad i = 1, 2, 3, \ldots, M \tag{16}$$

where $A_1, A_2, \ldots, A_M$ are computed based on the definition of the shape functions as follows:

$$\begin{aligned} &N_i^{(\varphi)} = 1 \text{ for } \varphi = \varphi_i \\ &N_i^{(\varphi)} = 0 \text{ for } \varphi = \varphi_1, \varphi_2, \ldots, \varphi_{i-1}, \varphi_{i+1}, \ldots, \varphi_M. \end{aligned} \tag{17}$$

Along θ, as stated earlier, circular shape functions are used according to [11, 15]. By selecting $N = 2^n$ nodes (n is a positive integer parameter) in a circle, shape functions are obtained as:

$$\begin{aligned} N_j^{\theta} = &\frac{1}{2^{n-1}}\cos\left(2^{n-2}\left(\theta - \frac{(j-1)\pi}{2^{n-1}}\right)\right) \\ &\times \left[1 + \cos\left(2^{n-2}\left(\theta - \frac{(j-1)\pi}{2^{n-1}}\right)\right)\right] \\ &\times \left[1 + \cos\left(2^{n-3}\left(\theta - \frac{(j-1)\pi}{2^{n-1}}\right)\right)\right] \\ &\ldots\left[1 + \cos\left(2^{0}\left(\theta - \frac{(j-1)\pi}{8}\right)\right)\right], \quad j = 1, 2, 3, \ldots, N. \end{aligned} \tag{18}$$

Finally, shape functions for nodes of the superelement are calculated by multiplying Eqs. (16) and (18) as follows:

$$\begin{aligned} &N_{i,j}(\theta, \varphi) = N_i^{\varphi} \times N_j^{\theta} \quad i = 1, 2, 3, \ldots, M; \\ &j = 1, 2, 3, \ldots, N. \end{aligned} \tag{19}$$

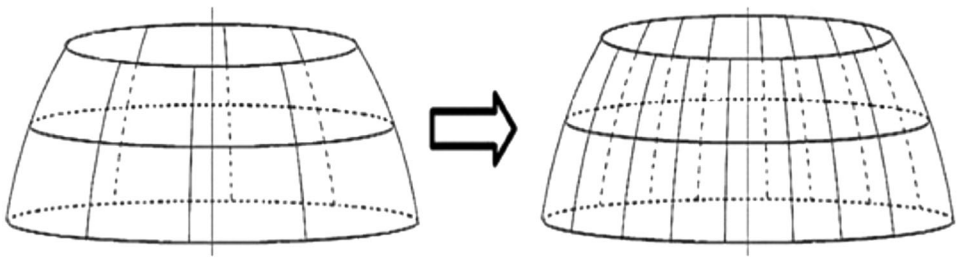

Fig. 6 Increasing the number of circumferential nodes in each superelement

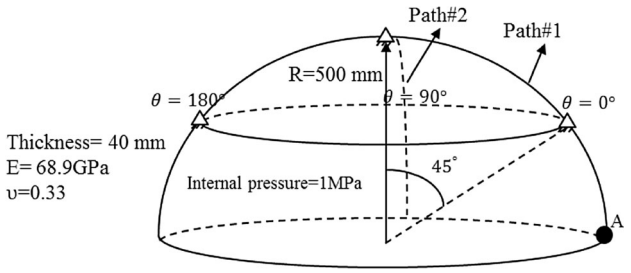

Fig. 7 The hemispherical shell in problem 1

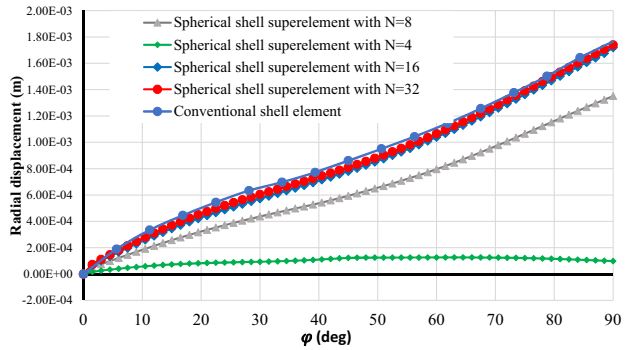

Fig. 8 Comparison of radial displacements in path #1

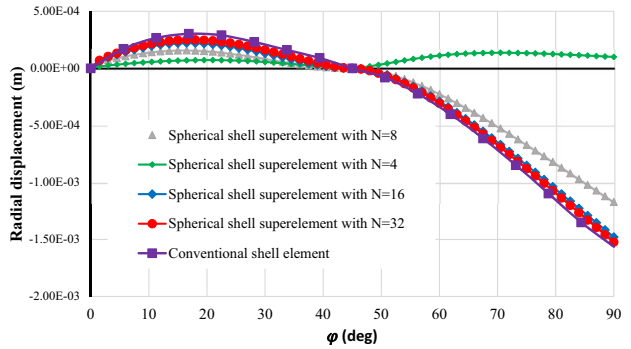

Fig. 9 Comparison of radial displacements in path #2

Table 1 Comparison of radial displacement at point A in problem 1

Parameter	Conventional shell elements	Spherical shell superelement (N = 16, M = 3)	Spherical shell superelement (N = 16, M = 2)
Radial displacement at point A (mm)	1.771	1.728	1.707
Number of elements	4238	20	50
Number of nodes	4342	641	801

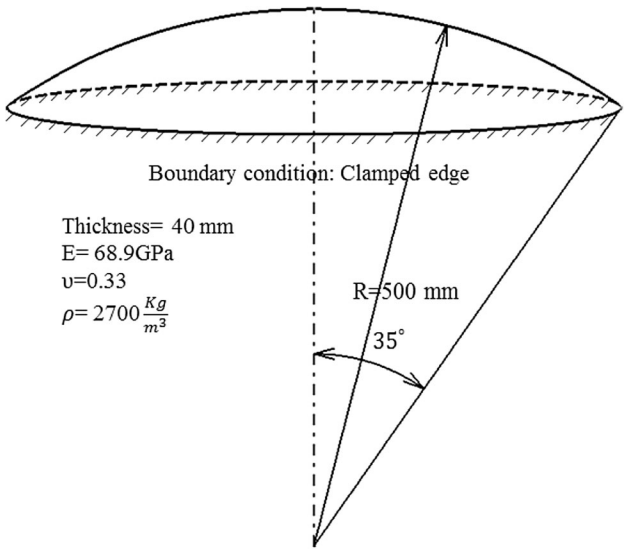

Fig. 10 The spherical shell in problem 2

Equation (19) is implemented for all nodes except for those which are poles ($\varphi = 0, \pi$). Shape functions in polar nodes are achieved by setting $N_j^{\theta} = 1$ in Eq. (19) since these points are individually located in the circumferential direction

In the presented shell superelement, the number of nodes is computed as below:

$$\begin{array}{ll} npe = 1 + N * (M-1) & \text{Shell superelement including pole} \\ npe = N * M & \text{Shell superelement without a pole} \end{array} \quad (20)$$

Figures 3 and 4 depict the general form of the obtained spherical shell superelement with M and N nodes in meridional and circumferential directions. The shape functions of these superelements for cases (1) $M = 2, N = 16$ and (2) $M = 3, N = 16$ can be found in Appendix 4.

By increasing the values of M and N, converging to the solution will be more time-consuming. On the other hand, decreasing these values can deteriorate the accuracy of results. Therefore, the optimum values of M and N should be selected, which will be discussed in Sects. 5.1 and 5.2 for static and vibration analysis of the spherical shells.

Figures 5 and 6 display how the accuracy of the finite element solution could be increased using this superelement. In Figs. 5 and 6, the accuracy will be improved due to increasing (a) the number of superelements and (b) the number of nodes in each superelement, respectively.

One of the most advantages of the presented superelement is that all axisymmetric shell structures can be discretized using this superelement. However, since the equations for spherical shells are presented in this study, this superelement is employed for analysis of the spherical shells.

Table 2 Comparison of the natural frequencies obtained by different N values in problem 2

Natural frequency	Conventional shell element (ANSYS) (4238 elements)		Spherical shell superelement with $N = 4$, $M = 2$ (100 elements)		Spherical shell superelement with $N = 8$, $M = 2$ (80 elements)		Spherical shell superelement with $N = 16$, $M = 2$ (50 elements)		Spherical shell superelement with $N = 32$, $M = 2$ (30 elements)	
	Result (rad/s)	Error (%)	Result (rad/s)	Error (%)	Result (rad/s)	Error (%)	Result (rad/s)	Error (%)	Result (rad/s)	Error (%)
ω_1	15,163	–	8104.1	46.553	15,151.2	0.077	15,158.4	0.031	15,159.1	0.026
ω_2	15,742	–	9265.9	41.138	16,089	2.204	15,722.0	0.127	15,720.6	0.136
ω_7	30,118	–	18,114.4	39.855	32,968.8	9.465	30,061.9	0.186	30,075.3	0.142
ω_{11}	37,295	–	22,285.4	40.245	39,684.5	6.407	37,860.9	1.517	37,866.2	1.518
ω_{18}	46,486	–	32,547.9	29.983	54,198.2	16.59	46,328.4	0.339	46,356.5	0.214

Table 3 Comparison of the natural frequencies obtained by different M values in problem 2

Natural frequency	Conventional shell element (ANSYS) (4238 elements)		Spherical shell superelement with $N = 16$, $M = 2$ (50 elements, 801 nodes)		Spherical shell superelement with $N = 16$, $M = 3$ (15 elements, 481 nodes)	
	Result (rad/s)	Error (%)	Result (rad/s)	Error (%)	Result (rad/s)	Error (%)
ω_1	15,163	–	15,158.4	0.031	15,157.5	0.036
ω_2	15,742	–	15,722	0.127	15,724.5	0.111
ω_7	30,118	–	30,061.9	0.186	30,100.5	0.058
ω_{11}	37,295	–	37,860.9	1.517	37,865.9	1.531
ω_{18}	46,486	–	46,328.4	0.339	46,405.5	0.173

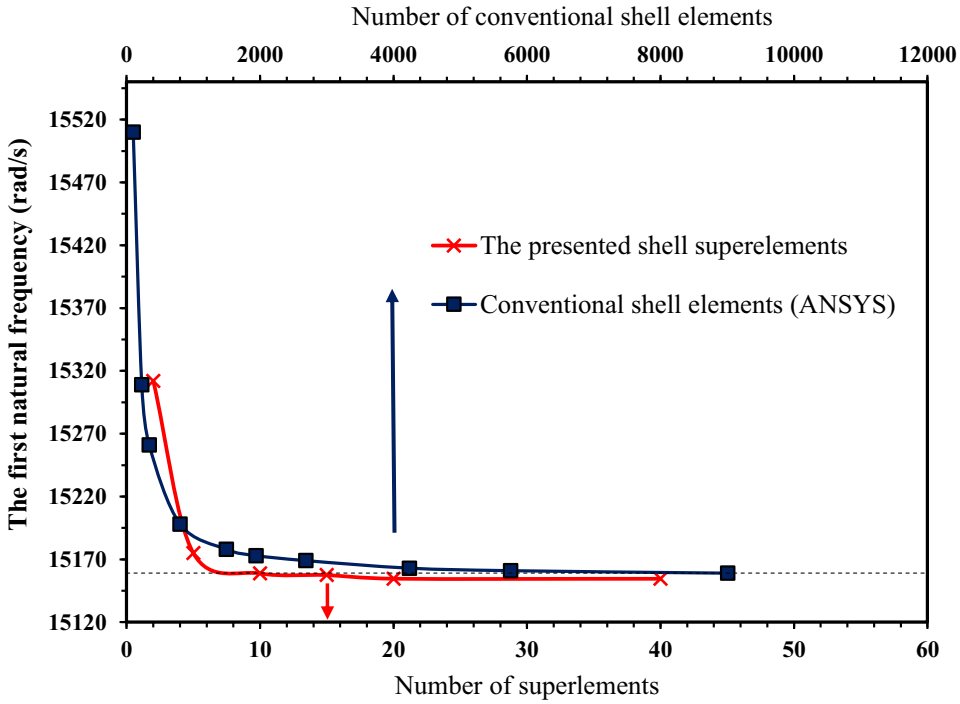

Fig. 11 Dependency of the first natural frequency to the number of conventional shell elements and shell superelements in problem 2

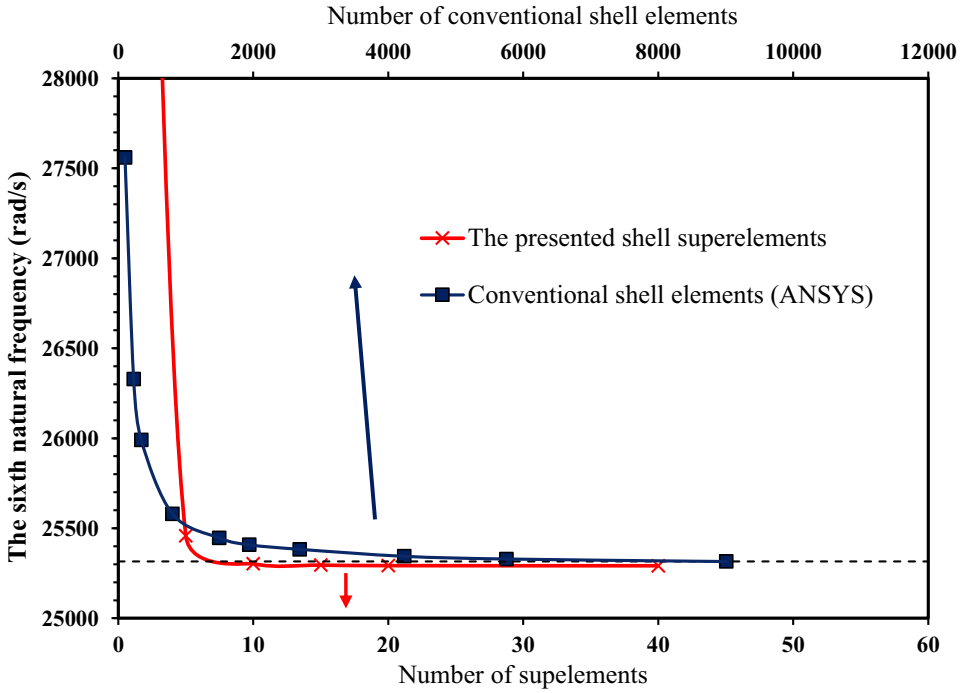

Fig. 12 Dependency of the sixth natural frequency to the number of conventional shell elements and shell superelements in problem 2

4.1 Coordinate transformation

The governing equations derived in Sect. 3 have been presented in terms of the global coordinates $(\varphi_1 \le \varphi \le \varphi_2, 0 \le \theta \le 2\pi)$. Since the numerical integration of the governing equations can be easily done using the local coordinate system $(-1 \le \gamma, \mu \le 1)$, conversion of global coordinates to local ones should be determined. In this research, the linear transformation and isoparametric mapping are employed to convert the global coordinates to the local ones in the circumferential and meridional directions, respectively, as given below:

$$\begin{aligned} &\theta = \pi(\mu+1), \quad 0 \le \theta \le 2\pi, \quad -1 \le \mu \le 1 \\ &\varphi = \sum_{i=1}^{npe} N_i(\gamma,\mu)\bar{\varphi}_i, \quad \varphi_1 \le \varphi \le \varphi_2, \quad -1 \le \gamma \le 1. \end{aligned} \tag{21}$$

Considering these mappings between global and local coordinates, the Jacobean matrix and infinitesimal area in the presented superelement are calculated as follows:

$$J = \begin{bmatrix} \frac{\partial\varphi}{\partial\gamma} & \frac{\partial\theta}{\partial\gamma} \\ \frac{\partial\varphi}{\partial\mu} & \frac{\partial\theta}{\partial\mu} \end{bmatrix} = \begin{bmatrix} \sum_{i=1}^{npe} \frac{\partial N_i(\gamma,\mu)}{\partial\gamma}\bar{\varphi}_i & 0 \\ \sum_{i=1}^{npe} \frac{\partial N_i(\gamma,\mu)}{\partial\mu}\bar{\varphi}_i & \pi \end{bmatrix}$$

$$\mathrm{d}A = R^2\sin(\varphi)\mathrm{d}\varphi\mathrm{d}\theta = \det(J)R^2\sin\left(\sum_{i=1}^{npe} N_i(\gamma,\mu)\bar{\varphi}_i\right)\mathrm{d}\gamma\mathrm{d}\mu \tag{22}$$

where $\bar{\varphi}$ represents the nodal values of the superelement in the meridional coordinate.

5 Results

In this section, several examples are presented to investigate the accuracy of the presented shell superelement under various types of loadings. In these problems, the achieved results using the offered shell superelement model are compared to the results obtained by using four-node shell elements of ANSYS software and also available results in the literature. In problems 1 and 2, static analysis and free vibration behavior of the isotropic spherical shell are studied and the optimum number of nodes and elements in

Table 4 Material properties of the studied composite spherical shell

Parameter	E_1 (GPa)	E_2 (GPa)	G_{12} (GPa)	G_{13} (GPa)	G_{23} (GPa)	$\nu_{12} = \nu_{21}$	ρ (kg/m^3)
Value	138	10.6	6	3.9	3.9	0.28	1500

Table 5 Comparison of the fundamental frequency parameter for different shell thicknesses and fiber orientations among all approaches

R/h	$(\omega_1 R\sqrt{\rho/E_2})$																	
	[0°]				[90°]				[0°/90°/0°]				[90°/0°/90°]					
	Present	ANSYS	Ref. [18]	Ref. [22]	Present	ANSYS	Ref. [18]	Ref. [22]	Present	ANSYS	Ref. [18]	Ref. [22]	Present	ANSYS	Ref. [18]	Ref. [22]	Present	ANSYS	Ref. [18]	Ref. [22]
100	0.874	0.879	0.884	0.880	0.0941	0.950	0.976	0.952	1.101	1.111	1.157	1.124	1.103	1.113	1.133	1.121	1.074	1.083	1.125	1.098
50	0.924	0.931	0.932	0.930	0.0945	0.952	0.978	0.954	1.138	1.146	1.183	1.154	1.151	1.159	1.180	1.165	1.101	1.108	1.145	1.121
20	1.116	1.125	1.130	1.122	0.0952	0.959	0.983	0.960	1.194	1.200	1.237	1.200	1.246	1.253	1.284	1.260	1.136	1.145	1.185	1.156
14.2	1.222	1.233	1.253	1.230	0.0961	0.964	0.988	0.965	1.214	1.223	1.263	1.215	1.291	1.300	1.340	1.305	1.148	1.159	1.202	1.168
10	1.325	1.335	1.386	1.328	0.0967	0.971	0.995	0.972	1.233	1.247	1.292	1.230	1.333	1.349	1.404	1.347	1.165	1.174	1.222	1.181

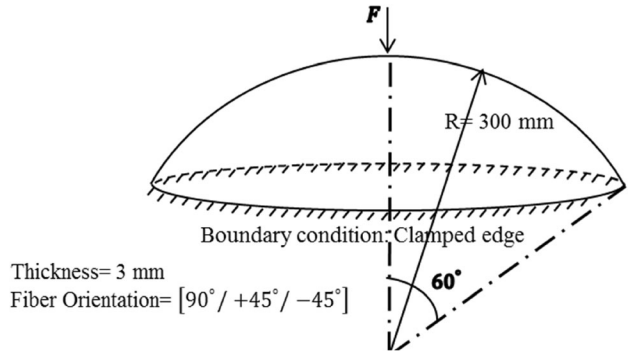

Fig. 13 The spherical shell in problem 4

the superelement model is obtained. In the next problems, free vibration and linear/nonlinear static analysis of composite spherical shells will be numerically investigated.

5.1 Problem 1

In this problem, the internal pressure of 1 MPa is applied to the hemispherical shell displayed in Fig. 7. The main objective of this problem is to find the optimum values of N and M (the number of nodes in the circumferential and meridional directions) in the presented shell superelement for static analysis of spherical shells. For this purpose, Figs. 8 and 9 illustrate the obtained radial displacements along φ direction in paths #1 and 2 by two different methods: (1) using the presented spherical shell superelement with varied values of N and (2) employing conventional shell elements of ANSYS software. Figures 8 and 9 show that setting $N = 4$ and 8 is not computationally accurate for this analysis, and the optimum value of N to obtain the acceptable accuracy results is 16. Also, the effects of considering two different values of M on the radial displacement at point A are investigated in Table 1. As presented in Table 1, $M = 2$ and $M = 3$ lead to a comparable accuracy, though setting $M = 3$ requires fewer elements and nodes. Therefore, this study recommends using the presented shell superelement with $N = 16$ and $M = 3$ for static analysis of spherical shells.

5.2 Problem 2

Vibration analysis of the spherical shell depicted in Fig. 10 is presented. The aims of this problem are (1) to evaluate the performance of the spherical shell superelement in the prediction of natural frequencies, (2) to investigate the required number of nodes in each spherical shell superelement and (3) to study the effects of superelement size on the solution accuracy.

Table 2 compares the natural frequencies obtained by conventional shell elements and different types of shell

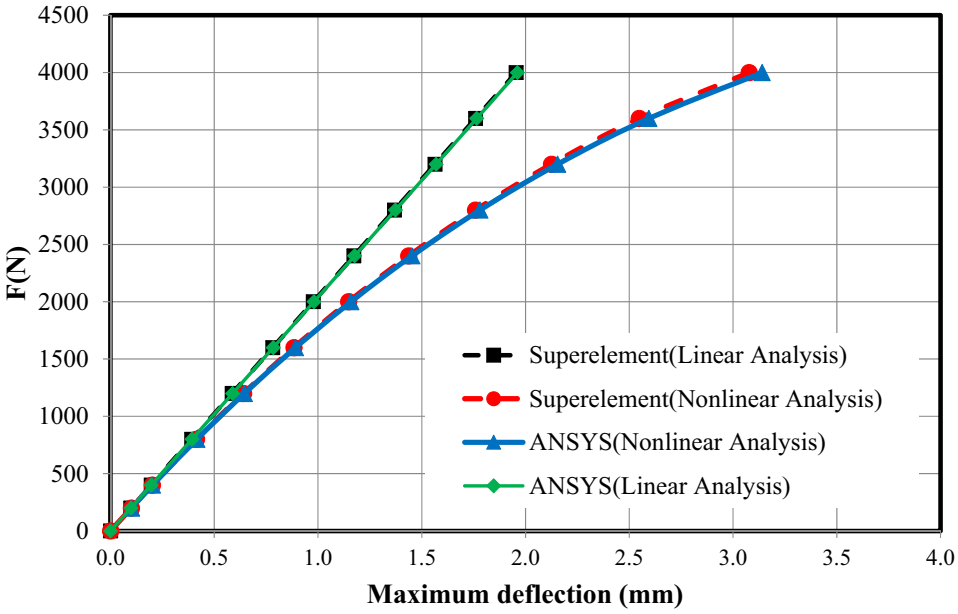

Fig. 14 Variations of displacement under the load versus the magnitude of the force

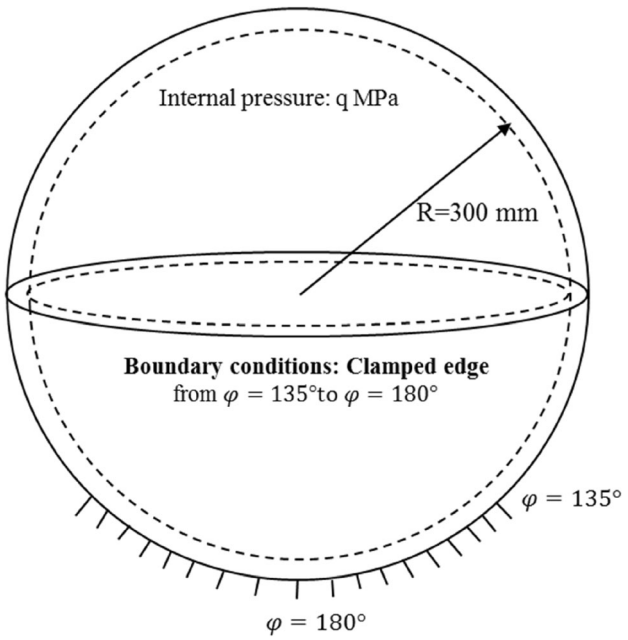

Fig. 15 Pressure vessel in problem 5

superelements. This table shows that using the spherical shell superelements with four and eight nodes in the θ direction cannot predict the natural frequencies of the studied shell accurately. On the other hand, although the accuracy of results cannot be meaningfully improved by employing $N = 32$, the solution time is significantly increased in this case. Therefore, similar to static analysis carried out in example 2, spherical shell superelements with $N = 16$ are selected for vibration analysis of the spherical shell. Furthermore, Table 3 compares the natural frequencies calculated by two different M values. As can be seen in Table 3, less number of elements and nodes is required for setting $M = 3$, while retaining the same level of accuracy. Therefore, the optimum values of N and M that minimize the solution time and maximize the result accuracy are obtained by setting $N = 16$ and $M = 3$ for vibration analysis of the spherical shells.

Figures 11 and 12 illustrate the dependency of the first and sixth natural frequencies of the studied shell to the number of conventional shell elements and shell superelements. As displayed in these figures, the number of required shell superelements for converging the solution is approximately 15 (481 nodes), while this number is about 4238 (4342 nodes) in the case of using conventional shell elements. Therefore, the number of required elements and nodes is significantly decreased when the problem is discretized via the presented shell superelement.

5.3 Problem 3

The main purpose of this problem is evaluating the performance of the composite spherical shell superelement in prediction of natural frequencies. For this purpose, free vibration analysis of a hemispherical shell ($R = 1000$ mm) with the boundary conditions $u_0 = v_0 = w_0 = \beta_\varphi = \beta_\theta = 0$ at the bottom edge and $u_0 = v_0 = \beta_\theta = 0$ at the apex is

Table 6 Comparing the maximum dimensionless radial displacement ($\frac{w_{max}}{h}$) in problem 5

q (Mpa)	R/h	$\left(\frac{w_{max}}{h}\right)$											
		[90°]			[45°]			[45°/ − 45°]			[90°/45°/ − 45°]		
		ANSYS (Shell)	Shell Superelement	3D Superelement	ANSYS (Shell)	Shell Superelement	3D Superelement	ANSYS (Shell)	Shell Superelement	3D Superelement	ANSYS (Shell)	Shell Superelement	3D Superelement
0.53	100	0.9047	0.9030	0.9282	0.1482	0.1473	0.1514	0.0491	0.0484	0.0501	0.2683	0.2670	0.2744
1.04	80	1.1048	1.1013	1.1313	0.1882	0.1871	0.1921	0.0635	0.0630	0.0642	0.3299	0.3286	0.3370
4.24	50	1.6568	1.6362	1.6767	0.3093	0.3073	0.3152	0.1094	0.1084	0.1117	0.5022	0.4975	0.5078
19.63	30	2.5770	2.5381	2.5861	0.5366	0.5332	0.5438	0.1999	0.1980	0.2024	0.7960	0.7881	0.8043

conducted for different shell thicknesses and fiber orientations. Material properties of this composite spherical shell are given in Table 4. In Table 5, fundamental natural frequency parameter ($\omega_1 R\sqrt{\rho/E_2}$) obtained by the composite spherical shell superelements is compared with the results presented in Refs. [18, 22] and conventional shell elements of ANSYS software. Results comparisons confirm the credibility of the composite spherical shell superelement in free vibration analysis.

5.4 Problem 4

The composite spherical shell displayed in Fig. 13 is subjected to the concentrated force (F). Material properties of this spherical shell are given in Table 4. Here, linear and nonlinear solutions are compared. Figure 14 shows the maximum deflection calculated by shell superelements and conventional shell elements for different values of F. As depicted in Fig. 14, by increasing the F value, the difference between the results obtained by linear and nonlinear solutions grows significantly. The achieved results indicate that the same trend and proper consistency are observed between the conventional shell element of ANSYS software and the presented shell superelement model in both linear and nonlinear solutions. The solution procedure for the nonlinear equations is given in Appendix 3.

5.5 Problem 5

The purpose of this problem is the linear static analysis of the composite spherical vessel shown in Fig. 15 with three different methods: using the proposed shell superelement, spherical superelements according to [15] and conventional shell elements of ANSYS software. Material properties of the used composite are given in Table 4. Since the spherical superelement developed in [15] is 3-dimensional, 3D elasticity equations are used to analyze the problem using this superelement. A total of 2524 shell elements in ANSYS, three spherical superelements with 228-node [15] and 16 spherical shell superelements with $N = 16$ and $M = 3$ of this work are employed to study this problem. Table 6 compares the maximum dimensionless radial displacement parameter ($\frac{w_{max}}{h}$) obtained by these methods for different fiber orientations, shell radius-to-thickness ratios (R/h) and internal pressures (q). In all simulations, the radius of the vessel (R) and dimensionless parameter $Q = \left(\frac{q}{E_2}\right) \times \left(\frac{R}{h}\right)^3$ are set as 300 mm and 50. Table 6 shows that high accuracy results are obtained in both superelement models. However, the required time for solving this problem using the proposed shell superelements is less, compared to 3D spherical superelements. This outcome is caused by the fewer Gaussian points in the presented shell superelements

Table 7 Comparison of natural frequencies in problem 6

Thickness = 0.125 in. Radius = 6 in.	Experiment [44]		Superelement model	
	Value (rad/s)	Error (%)	Value (rad/s)	Error (%)
1st asymmetric natural frequency	7300	–	7464	2.20
2nd asymmetric natural frequency	9300	–	9402	1.08
3rd asymmetric natural frequency	11,900	–	12,183	2.32
4th asymmetric natural frequency	15,200	–	15,631	2.76
5th asymmetric natural frequency	19,100	–	19,701	3.05

compared to the 3D spherical superelement. Therefore, by employing the presented shell superelement, the mechanical behavior of spherical vessels can be studied with a high level of accuracy and decreased computational cost.

It should be noted that the detailed information regarding the required number of Gaussian points in the spherical superelement can be found in Ref. [15].

5.6 Problem 6

The purpose of this problem is to evaluate the accuracy of the presented superelement model in comparison with the experimental results reported in Ref. [44]. In this problem, asymmetrical natural frequencies of a steel shallow spherical shell with clamped boundary conditions are studied. The material properties and geometry parameters of this spherical shell are given in Ref. [44]. Table 7 presents the asymmetrical natural frequencies resulted from experiment and the present shell superelement model. Comparisons of natural frequencies indicate the credibility of the superelement model, with the maximum error between the superelement model and experiment being around 3%.

6 Conclusions

In this paper, a new shell superelement for finite element analysis of spherical shell structures has been presented. This superelement deals with the first-order shear deformation theory and considering large deformation formulation. Comparing the results between the proposed shell superelement and conventional shell elements reveals that this superelement is capable of predicting structural, vibratory and nonlinear behavior of the spherical shell with high accuracy and decreased computational costs. Several significant properties obtained by the presented shell superelement are summarized as follows:

- The presented superelement can analyze partial spherical sectors with and without apex and complete spherical shells properly;
- For static and vibration analysis of spherical shells, the optimum number of nodes in each superelement is obtained by setting $M = 3$ and $N = 16$ resulting in 48-node superelement without apex and 33-node superelement with apex;
- In the mechanical analysis of the spherical vessels, employing the presented shell superelement is much more computationally efficient than that of the 3D spherical superelement presented in the literature, at the comparable level of accuracy;
- The presented superelement predicts the behavior of spherical shells under local loads and boundary conditions with acceptable level of accuracy.

Appendix 1

$[B_m], [B_b], [B_s]$ and $[B_{NL}]$ are given as the following equations:

$$
\begin{aligned}
[B_m] &= \begin{bmatrix}
\frac{1}{R}\frac{\partial N_1}{\partial \varphi} & 0 & \frac{1}{R}N_1 & 0 & 0 & \ldots & \frac{1}{R}\frac{\partial N_i}{\partial \varphi} & 0 & \frac{1}{R}N_1 & 0 & 0 \\
\frac{\cot(\varphi)}{R}N_1 & \frac{1}{R\sin(\varphi)}\frac{\partial N_1}{\partial \theta} & \frac{1}{R}N_1 & 0 & 0 & \ldots & \frac{\cot(\varphi)}{R}N_i & \frac{1}{R\sin(\varphi)}\frac{\partial N_i}{\partial \theta} & \frac{1}{R}N_1 & 0 & 0 \\
\frac{1}{R\sin(\varphi)}\frac{\partial N_1}{\partial \theta} & \frac{1}{R}\frac{\partial N_1}{\partial \varphi} - \frac{\cot(\varphi)}{R}N_1 & 0 & 0 & 0 & \ldots & \frac{1}{R\sin(\varphi)}\frac{\partial N_i}{\partial \theta} & \frac{1}{R}\frac{\partial N_i}{\partial \varphi} - \frac{\cot(\varphi)}{R}N_i & 0 & 0 & 0
\end{bmatrix} \\
[B_b] &= \begin{bmatrix}
0 & 0 & 0 & \frac{1}{R}\frac{\partial N_1}{\partial \varphi} & 0 & \ldots & 0 & 0 & 0 & \frac{1}{R}\frac{\partial N_i}{\partial \varphi} & 0 \\
0 & 0 & 0 & \frac{\cot(\varphi)}{R}N_1 & \frac{1}{R\sin(\varphi)}\frac{\partial N_1}{\partial \theta} & \ldots & 0 & 0 & 0 & \frac{\cot(\varphi)}{R}N_i & \frac{1}{R\sin(\varphi)}\frac{\partial N_i}{\partial \theta} \\
0 & 0 & 0 & \frac{1}{R\sin(\varphi)}\frac{\partial N_1}{\partial \theta} & \frac{1}{R}\frac{\partial N_1}{\partial \varphi} - \frac{\cot(\varphi)}{R}N_1 & \ldots & 0 & 0 & 0 & \frac{1}{R\sin(\varphi)}\frac{\partial N_i}{\partial \theta} & \frac{1}{R}\frac{\partial N_i}{\partial \varphi} - \frac{\cot(\varphi)}{R}N_i
\end{bmatrix} \\
[B_s] &= \begin{bmatrix}
-\frac{1}{R}N_1 & 0 & \frac{1}{R}\frac{\partial N_1}{\partial \varphi} & 1 & 0 \ldots & -\frac{1}{R}N_i & 0 & \frac{1}{R}\frac{\partial N_i}{\partial \varphi} & 1 & 0 \\
0 & -\frac{1}{R}N_1 & \frac{1}{R\sin(\varphi)}\frac{\partial N_1}{\partial \theta} & 0 & 1 \ldots & 0 & -\frac{1}{R}N_i & \frac{1}{R\sin(\varphi)}\frac{\partial N_i}{\partial \theta} & 0 & 1
\end{bmatrix}
\end{aligned} \tag{23}
$$

$$
[B_{NL}] = \begin{bmatrix} B_{NL}^{(1)} \\ B_{NL}^{(2)} \\ B_{NL}^{(3)} \end{bmatrix} = \begin{Bmatrix} \frac{1}{2}\{U\}^T\{\tilde{d}_1\}^T\{\tilde{d}_1\} \\ \frac{1}{2}\{U\}^T\{\tilde{d}_2\}^T\{\tilde{d}_2\} \\ \frac{1}{2}\{U\}^T\{\tilde{d}_1\}^T\{\tilde{d}_2\} \end{Bmatrix}
$$

$$
[B_{NL}] = \begin{bmatrix}
\frac{1}{2R^2}\left\{0 \quad 0 \quad \frac{\partial N_1}{\partial \varphi}\sum_{i=1}^{npe}\frac{\partial N_i}{\partial \varphi}w_i \quad 0 \quad 0 \quad \ldots \quad \ldots \quad 0 \quad 0 \quad \frac{\partial N_{npe}}{\partial \varphi}\sum_{i=1}^{npe}\frac{\partial N_i}{\partial \varphi}w_i \quad 0 \quad 0\right\} \\
\frac{1}{2R^2\sin^2(\varphi)}\left\{0 \quad 0 \quad \frac{\partial N_1}{\partial \theta}\sum_{i=1}^{npe}\frac{\partial N_i}{\partial \theta}w_i \quad 0 \quad 0 \quad \ldots \quad \ldots \quad 0 \quad 0 \quad \frac{\partial N_{npe}}{\partial \theta}\sum_{i=1}^{npe}\frac{\partial N_i}{\partial \theta}w_i \quad 0 \quad 0\right\} \\
\frac{1}{R^2\sin(\varphi)}\left\{0 \quad 0 \quad \frac{\partial N_1}{\partial \theta}\sum_{i=1}^{npe}\frac{\partial N_i}{\partial \varphi}w_i \quad 0 \quad 0 \quad \ldots \quad \ldots \quad 0 \quad 0 \quad \frac{\partial N_{npe}}{\partial \theta}\sum_{i=1}^{npe}\frac{\partial N_i}{\partial \varphi}w_i \quad 0 \quad 0\right\}.
\end{bmatrix}
$$

Appendix 2

$K_1, K_2, K_3, \ldots, K_{10}$ are specified as the following equations:

$$
\begin{aligned}
K_1 &= \iint_{A^e} [B_m]^T [A][B_m] \mathrm{d}A \\
K_2 &= \iint_{A^e} [B_m]^T [A][B_{NL}] \mathrm{d}A \\
K_3 &= \iint_{A^e} [B_m]^T [B][B_b] \mathrm{d}A \\
K_4 &= \iint_{A^e} \left[\tilde{B}_{NL}\right]^T [A][B_m] \mathrm{d}A \\
K_5 &= \iint_{A^e} \left[\tilde{B}_{NL}\right]^T [A][B_{NL}] \mathrm{d}A \\
K_6 &= \iint_{A^e} \left[\tilde{B}_{NL}\right]^T [B][B_b] \mathrm{d}A \\
K_7 &= \iint_{A^e} [B_b]^T [B][B_m] dA \\
K_8 &= \iint_{A^e} [B_b]^T [B][B_{NL}] dA \\
K_9 &= \iint_{A^e} [B_b]^T [D][B_b] \mathrm{d}A \\
K_{10} &= \iint_{A^e} [B_s]^T [A_s][B_s] \mathrm{d}A.
\end{aligned} \tag{24}
$$

In the above equation, $\left[\tilde{B}_{NL}\right]$ is written as:

$$
\left[\tilde{B}_{NL}\right] = \begin{bmatrix} \tilde{B}_{NL}^{(1)} \\ \tilde{B}_{NL}^{(2)} \\ \tilde{B}_{NL}^{(3)} \end{bmatrix}
$$

$$
\begin{aligned}
\tilde{B}_{NL}^{(1)} &= \frac{1}{R^2} \left\{ 0 \quad 0 \quad \frac{\partial N_1}{\partial \varphi} \sum_{i=1}^{npe} \frac{\partial N_i}{\partial \varphi} w_i \quad 0 \quad 0 \quad \cdots \quad \cdots 0 \quad 0 \right. \\
&\quad \left. \times \frac{\partial N_{npe}}{\partial \varphi} \sum_{i=1}^{npe} \frac{\partial N_i}{\partial \varphi} w_i \quad 0 \quad 0 \right\} \\
\tilde{B}_{NL}^{(2)} &= \frac{1}{R^2 \sin^2(\varphi)} \\
&\quad \times \left\{ 0 \quad 0 \quad \frac{\partial N_1}{\partial \theta} \sum_{i=1}^{npe} \frac{\partial N_i}{\partial \theta} w_i \quad 0 \quad 0 \quad \ldots \quad \ldots \quad 0 \quad 0 \right. \\
&\quad \left. \times \frac{\partial N_{npe}}{\partial \theta} \sum_{i=1}^{npe} \frac{\partial N_i}{\partial \theta} w_i \quad 0 \quad 0 \right\}
\end{aligned}
$$

$$
\begin{aligned}
\tilde{B}_{NL}^{(3)} &= \frac{1}{R^2 \sin(\varphi)} \left\{ 0 \quad 0 \quad \left(\frac{\partial N_1}{\partial \theta} \sum_{i=1}^{npe} \frac{\partial N_i}{\partial \varphi} w_i \right) \right. \\
&\quad \times + \left(\frac{\partial N_1}{\partial \varphi} \sum_{i=1}^{npe} \frac{\partial N_i}{\partial \theta} w_i \right) \quad 0 \quad 0 \quad \ldots \quad \ldots \quad 0 \quad 0 \\
&\quad \left. \times \left(\frac{\partial N_{npe}}{\partial \theta} \sum_{i=1}^{npe} \frac{\partial N_i}{\partial \varphi} w_i \right) + \left(\frac{\partial N_{npe}}{\partial \varphi} \sum_{i=1}^{npe} \frac{\partial N_i}{\partial \theta} w_i \right) \quad 0 \quad 0 \right\}.
\end{aligned} \tag{25}
$$

Appendix 3

This research uses the Newton–Raphson algorithm for solving the nonlinear governing equation as follows:

$$
\begin{aligned}
&[K^t(\{U\}^r)]\{\Delta U\} = \{F\} - [K(\{U\}^r)]\{U\}^r \\
&\{U\}^{r+1} = \{U\}^r + \{\Delta U\}
\end{aligned} \tag{26}
$$

where K^t is the tangent stiffness matrix which is expressed as follows:

$$
(K_{ij}^t)^r = K_{ik,j}^r U_k^r + K_{ij}^r \tag{27}
$$

where

$$
\begin{aligned}
&K_{ik,j}^r = (K_2)_{ik,j}^r + (K_4)_{ik,j}^r + (K_5)_{ik,j}^r + (K_6)_{ik,j}^r + (K_8)_{ik,j}^r \\
&(K_2)_{ik,j}^r = (B_m)_{pi} (A)_{pq} (B_{NL})_{qk,j} \\
&(K_4)_{ik,j}^r = \left(\tilde{B}_{NL}\right)_{pi,j} (A)_{pq} (B_m)_{qk,j} \\
&(K_5)_{ik,j}^r = \left(\tilde{B}_{NL}\right)_{pi,j} (A)_{pq} (B_{NL})_{qk}^r + \left(\tilde{B}_{NL}\right)_{pi}^r (A)_{pq} (B_{NL})_{qk,j} \\
&(K_6)_{ik,j} = \left(\tilde{B}_{NL}\right)_{pi,j} (B)_{pq} (B_b)_{qk} \\
&(K_8)_{ik,j} = (B_b)_{pi} (B)_{pq} (B_{NL})_{q,jk} \\
&\quad i,j,k = 1 : dof \times npe; \quad p,q = 1,2,3.
\end{aligned} \tag{28}
$$

Nonzero terms of $(B_{NL})_{pi,j}$ and $\left(\tilde{B}_{NL}\right)_{pi,j}$ matrices are defined as the following equations:

$$
(B_{NL})_{pi,j} = \begin{Bmatrix} [B_{NL}]_{1i,j} \\ [B_{NL}]_{2i,j} \\ [B_{NL}]_{3i,j} \end{Bmatrix}, \left(\tilde{B}_{NL}\right)_{pi,j} = \begin{Bmatrix} \left[\tilde{B}_{NL}\right]_{1i,j} \\ \left[\tilde{B}_{NL}\right]_{2i,j} \\ \left[\tilde{B}_{NL}\right]_{3i,j} \end{Bmatrix} \tag{29}
$$

where

$$[B_{NL}]_{1i,j}=\begin{bmatrix} B^{11}_{1NLj} & B^{12}_{1NLj} & \cdots & B^{1l}_{1NLj} \\ B^{21}_{1NLj} & B^{22}_{1NLj} & \cdots & B^{1l}_{1NLj} \\ \vdots & \vdots & \ddots & \vdots \\ B^{k1}_{1NLj} & B^{k2}_{1NLj} & \cdots & B^{kl}_{1NLj} \end{bmatrix},\quad [\tilde{B}_{NL}]_{1i,j}=\begin{bmatrix} \tilde{B}^{11}_{1NLj} & \tilde{B}^{12}_{1NLj} & \cdots & \tilde{B}^{1l}_{1NLj} \\ \tilde{B}^{21}_{1NLj} & \tilde{B}^{22}_{1NLj} & \cdots & \tilde{B}^{1l}_{1NLj} \\ \vdots & \vdots & \ddots & \vdots \\ \tilde{B}^{k1}_{1NLj} & \tilde{B}^{k2}_{1NLj} & \cdots & \tilde{B}^{kl}_{1NLj} \end{bmatrix}$$

$$[B_{NL}]_{2i,j}=\begin{bmatrix} B^{11}_{2NLj} & B^{12}_{2NLj} & \cdots & B^{1l}_{2NLj} \\ B^{21}_{2NLj} & B^{22}_{2NLj} & \cdots & B^{1l}_{2NLj} \\ \vdots & \vdots & \ddots & \vdots \\ B^{k1}_{2NLj} & B^{k2}_{2NLj} & \cdots & B^{kl}_{2NLj} \end{bmatrix},\quad [\tilde{B}_{NL}]_{2i,j}=\begin{bmatrix} \tilde{B}^{11}_{2NLj} & \tilde{B}^{12}_{2NLj} & \cdots & \tilde{B}^{1l}_{2NLj} \\ \tilde{B}^{21}_{2NLj} & \tilde{B}^{22}_{2NLj} & \cdots & \tilde{B}^{1l}_{2NLj} \\ \vdots & \vdots & \ddots & \vdots \\ \tilde{B}^{k1}_{2NLj} & \tilde{B}^{k2}_{2NLj} & \cdots & \tilde{B}^{kl}_{2NLj} \end{bmatrix}$$

$$[B_{NL}]_{3i,j}=\begin{bmatrix} B^{11}_{3NLj} & B^{12}_{3NLj} & \cdots & B^{1l}_{3NLj} \\ B^{21}_{3NLj} & B^{22}_{3NLj} & \cdots & B^{1l}_{3NLj} \\ \vdots & \vdots & \ddots & \vdots \\ B^{k1}_{3NLj} & B^{k2}_{3NLj} & \cdots & B^{kl}_{3Lj} \end{bmatrix},$$

$$[\tilde{B}_{NL}]_{3i,j}=\begin{bmatrix} \tilde{B}^{11}_{3NLj} & \tilde{B}^{12}_{3NLj} & \cdots & \tilde{B}^{1l}_{3NLj} \\ \tilde{B}^{21}_{3NLj} & \tilde{B}^{22}_{3NLj} & \cdots & \tilde{B}^{1l}_{3NLj} \\ \vdots & \vdots & \ddots & \vdots \\ \tilde{B}^{k1}_{3NLj} & \tilde{B}^{k2}_{3NLj} & \cdots & \tilde{B}^{kl}_{3NLj} \end{bmatrix}$$

$$B^{kl}_{1NLJ}=\frac{1}{2R^2}\begin{bmatrix} 0 & 0 & 0 & 0 & 0 \\ 0 & 0 & 0 & 0 & 0 \\ 0 & 0 & N_{k,\varphi}N_{l,\varphi} & 0 & 0 \\ 0 & 0 & 0 & 0 & 0 \\ 0 & 0 & 0 & 0 & 0 \end{bmatrix},\quad \tilde{B}^{kl}_{1NLJ}=\frac{1}{R^2}\begin{bmatrix} 0 & 0 & 0 & 0 & 0 \\ 0 & 0 & 0 & 0 & 0 \\ 0 & 0 & N_{k,\varphi}N_{l,\varphi} & 0 & 0 \\ 0 & 0 & 0 & 0 & 0 \\ 0 & 0 & 0 & 0 & 0 \end{bmatrix}$$

$$B^{kl}_{2NLJ}=\frac{1}{2R^2\sin^2(\varphi)}\begin{bmatrix} 0 & 0 & 0 & 0 & 0 \\ 0 & 0 & 0 & 0 & 0 \\ 0 & 0 & N_{k,\theta}N_{l,\theta} & 0 & 0 \\ 0 & 0 & 0 & 0 & 0 \\ 0 & 0 & 0 & 0 & 0 \end{bmatrix},$$

$$\tilde{B}^{kl}_{2NLJ}=\frac{1}{R^2\sin^2(\varphi)}\begin{bmatrix} 0 & 0 & 0 & 0 & 0 \\ 0 & 0 & 0 & 0 & 0 \\ 0 & 0 & N_{k,\theta}N_{l,\theta} & 0 & 0 \\ 0 & 0 & 0 & 0 & 0 \\ 0 & 0 & 0 & 0 & 0 \end{bmatrix}$$

$$B^{kl}_{3NLJ}=\frac{1}{R^2\sin(\varphi)}\begin{bmatrix} 0 & 0 & 0 & 0 & 0 \\ 0 & 0 & 0 & 0 & 0 \\ 0 & 0 & N_{k,\theta}N_{l,\varphi} & 0 & 0 \\ 0 & 0 & 0 & 0 & 0 \\ 0 & 0 & 0 & 0 & 0 \end{bmatrix},$$

$$\tilde{B}^{kl}_{3NLJ}=\frac{1}{R^2\sin(\varphi)}\begin{bmatrix} 0 & 0 & 0 & 0 & 0 \\ 0 & 0 & 0 & 0 & 0 \\ 0 & 0 & N_{k,\theta}N_{l,\varphi}+N_{k,\varphi}N_{l,\theta} & 0 & 0 \\ 0 & 0 & 0 & 0 & 0 \\ 0 & 0 & 0 & 0 & 0 \end{bmatrix}. \tag{30}$$

Appendix 4

Shape functions of the spherical shell superelement including pole in the local coordinate system are expressed as follows:

(a) $M = 3, N = 16$:

$$\begin{aligned} N_i &= \frac{\gamma(\gamma-1)}{2} \quad i=1 \\ N_{2,i} &= \frac{(1-\gamma)(1+\gamma)}{4}\times\cos\left(4\left(\pi(\mu+1)-\frac{(i-1)\times\pi}{8}\right)\right) \\ &\quad\times\left[1+\cos\left(4\left(\pi(\mu+1)-\frac{(i-1)\times\pi}{8}\right)\right)\right] \qquad i=1-16 \\ &\quad\times\left[1+\cos\left(2\left(\pi(\mu+1)-\frac{(i-1)\times\pi}{8}\right)\right)\right] \\ &\quad\times\left[1+\cos\left(\pi(\mu+1)-\frac{(i-1)\times\pi}{8}\right)\right] \\ N_{3,i} &= \frac{\gamma(\gamma+1)}{8}\times\cos\left(4\left(\pi(\mu+1)-\frac{(i-1)\times\pi}{8}\right)\right) \\ &\quad\times\left[1+\cos\left(4\left(\pi(\mu+1)-\frac{(i-1)\times\pi}{8}\right)\right)\right] \qquad i=1-16 \\ &\quad\times\left[1+\cos\left(2\left(\pi(\mu+1)-\frac{(i-1)\times\pi}{8}\right)\right)\right] \\ &\quad\times\left[1+\cos\left(\pi(\mu+1)-\frac{(i-1)\times\pi}{8}\right)\right] \end{aligned} \tag{31}$$

(b) $M = 2, N = 16$:

$$\begin{aligned} N_i &= \frac{(1-\lambda)}{2} \quad i=1 \\ N_{2,i} &= \frac{(1+\lambda)}{16}\times\cos\left(4\left(\pi(\mu+1)-\frac{(i-1)\times\pi}{8}\right)\right) \\ &\quad\times\left[1+\cos\left(4\left(\pi(\mu+1)-\frac{(i-1)\times\pi}{8}\right)\right)\right] \qquad i=1-16 \\ &\quad\times\left[1+\cos\left(2\left(\pi(\mu+1)-\frac{(i-1)\times\pi}{8}\right)\right)\right] \\ &\quad\times\left[1+\cos\left(\pi(\mu+1)-\frac{(i-1)\times\pi}{8}\right)\right] \end{aligned} \tag{32}$$

Also, the shape functions of the spherical shell superelement without pole are given as follows:

(a) $M = 3, N = 16$:

$$
\begin{aligned}
N_{1,i} &= \frac{\gamma(\gamma-1)}{8}\times\cos\left(4\left(\pi(\mu+1)-\frac{(i-1)\times\pi}{8}\right)\right)\\
&\times\left[1+\cos\left(4\left(\pi(\mu+1)-\frac{(i-1)\times\pi}{8}\right)\right)\right]\\
&\times\left[1+\cos\left(2\left(\pi(\mu+1)-\frac{(i-1)\times\pi}{8}\right)\right)\right]\\
&\times\left[1+\cos\left(\pi(\mu+1)-\frac{(i-1)\times\pi}{8}\right)\right]\\
N_{2,i} &= \frac{(1-\gamma)(1+\gamma)}{4}\times\cos\left(4\left(\pi(\mu+1)-\frac{(i-1)\times\pi}{8}\right)\right)\\
&\times\left[1+\cos\left(4\left(\pi(\mu+1)-\frac{(i-1)\times\pi}{8}\right)\right)\right]\\
&\times\left[1+\cos\left(2\left(\pi(\mu+1)-\frac{(i-1)\times\pi}{8}\right)\right)\right]\\
&\times\left[1+\cos\left(\pi(\mu+1)-\frac{(i-1)\times\pi}{8}\right)\right]\\
N_{3,i} &= \frac{\gamma(\gamma+1)}{8}\times\cos\left(4\left(\pi(\mu+1)-\frac{(i-1)\times\pi}{8}\right)\right)\\
&\times\left[1+\cos\left(4\left(\pi(\mu+1)-\frac{(i-1)\times\pi}{8}\right)\right)\right]\\
&\times\left[1+\cos\left(2\left(\pi(\mu+1)-\frac{(i-1)\times\pi}{8}\right)\right)\right]\\
&\times\left[1+\cos\left(\pi(\mu+1)-\frac{(i-1)\times\pi}{8}\right)\right]
\end{aligned}
\qquad i=1-16 \tag{33}
$$

(b) $M=2, N=16$:

$$
\begin{aligned}
N_{1,i} &= \frac{(1-\lambda)}{16}\times\cos\left(4\left(\pi(\mu+1)-\frac{(i-1)\times\pi}{8}\right)\right)\\
&\times\left[1+\cos\left(4\left(\pi(\mu+1)-\frac{(i-1)\times\pi}{8}\right)\right)\right]\\
&\times\left[1+\cos\left(2\left(\pi(\mu+1)-\frac{(i-1)\times\pi}{8}\right)\right)\right]\\
&\times\left[1+\cos\left(\pi(\mu+1)-\frac{(i-1)\times\pi}{8}\right)\right]\\
N_{2,i} &= \frac{(1+\lambda)}{16}\times\cos\left(4\left(\pi(\mu+1)-\frac{(i-1)\times\pi}{8}\right)\right)\\
&\times\left[1+\cos\left(4\left(\pi(\mu+1)-\frac{(i-1)\times\pi}{8}\right)\right)\right]\\
&\times\left[1+\cos\left(2\left(\pi(\mu+1)-\frac{(i-1)\times\pi}{8}\right)\right)\right]\\
&\times\left[1+\cos\left(\pi(\mu+1)-\frac{(i-1)\times\pi}{8}\right)\right]
\end{aligned}
\qquad i=1-16 \tag{34}
$$

References

1. Habibi M et al (2017) Determination of forming limit diagram using two modified finite element models. Amirkabir J Mech Eng 48:379–388. https://doi.org/10.22060/mej.2016.664
2. Kung E, Farahmand M, Gupta A (2019) A hybrid experimental–computational modeling framework for cardiovascular device testing. J Biomech Eng. https://doi.org/10.1115/1.4042665
3. Hughes TJR, Cottrell JA, Bazilevs Y (2005) Isogeometric analysis: CAD, finite elements, NURBS, exact geometry and mesh refinement. Comput Methods Appl Mech Eng 194:4135–4195. https://doi.org/10.1016/j.cma.2004.10.008
4. Nguyen LB, Thai CH, Nguyen-Xuan H (2016) A generalized unconstrained theory and isogeometric finite element analysis based on Bézier extraction for laminated composite plates. Eng Comput 32:457–475. https://doi.org/10.1007/s00366-015-0426-x
5. Shamloofard M, Assempour A (2019) Development of an inverse isogeometric methodology and its application in sheet metal forming process. Appl Math Model 73:266–284. https://doi.org/10.1016/j.apm.2019.03.042
6. Koko TS, Olson MD (1991) Non-linear analysis of stiffened plates using super elements. Int J Numer Methods Eng 31:319–343. https://doi.org/10.1002/nme.1620310208
7. Koko TS, Olson MD (1991) Nonlinear transient response of stiffened plates to air blast loading by a superelement approach. Comput Methods Appl Mech Eng 90:737–760. https://doi.org/10.1016/0045-7825(91)90182-6
8. Koko TS, Olson MD (1992) Vibration analysis of stiffened plates by super elements. J Sound Vib 158:149–167. https://doi.org/10.1016/0022-460X(92)90670-S
9. Jiang J, Olson MD (1994) Nonlinear analysis of orthogonally stiffened cylindrical shells by a super element approach. Finite Elem Anal Des 18:99–110. https://doi.org/10.1016/0168-874X(94)90094-9
10. Ahmadian MT, Zangeneh M (2003) Application of super elements to free vibration analysis of laminated stiffened plates. J Sound Vib 259:1243–1252. https://doi.org/10.1006/jsvi.2002.5288
11. Ahmadian MT, Bonakdar M (2008) A new cylindrical element formulation and its application to structural analysis of laminated hollow cylinders. Finite Elem Anal Des 44:617–630. https://doi.org/10.1016/j.finel.2008.02.003
12. Ahmadian MT, Movahhedy MR, Rezaei MM (2011) Design and application of a new tapered superelement for analysis of revolving geometries. Finite Elem Anal Des 47:1242–1252. https://doi.org/10.1016/j.finel.2011.06.002
13. Torabi J, Ansari R (2018) A higher-order isoparametric superelement for free vibration analysis of functionally graded shells of revolution. Thin Walled Struct 133:169–179. https://doi.org/10.1016/j.tws.2018.09.040
14. Sarvi MN, Ahmadian MT (2012) Design and implementation of a new spherical super element in structural analysis. Appl Math Comput 218:7546–7561. https://doi.org/10.1016/j.amc.2012.01.022
15. Shamloofard M, Movahhedy MR (2015) Development of thermo-elastic tapered and spherical superelements. Appl Math Comput 265:380–399. https://doi.org/10.1016/j.amc.2015.04.106
16. Dhari RS, Patel NP, Wang H, Hazell PJ (2019) Progressive damage modeling and optimization of fibrous composites under ballistic impact loading. Mech Adv Mater Struct. https://doi.org/10.1080/15376494.2019.1655688
17. Habibi M et al (2019) Wave propagation analysis of the laminated cylindrical nanoshell coupled with a piezoelectric actuator. Mech Based Des Struct Mach. https://doi.org/10.1080/15397734.2019.1697932
18. Gautham BP, Ganesan N (1997) Free vibration characteristics of isotropic and laminated orthotropic spherical caps. J Sound Vib 204:17–40. https://doi.org/10.1006/jsvi.1997.0904
19. Ram KSS, Babu TS (2002) Free vibration of composite spherical shell cap with and without a cutout. Comput Struct 80:1749–1756. https://doi.org/10.1016/S0045-7949(02)00210-9
20. Pang F, Li H, Cuib J, Du Y, Gao C (2019) Application of flügge thin shell theory to the solution of free vibration behaviors for spherical–cylindrical–spherical shell: a unified formulation. Eur J Mech A Solids 74:381–393. https://doi.org/10.1016/j.euromechsol.2018.12.003
21. Hosseini-Hashemi Sh, Atashipour SR, Fadaee M, Girjammer UA (2012) An exact closed-form procedure for free vibration analysis of laminated spherical shell panels based on Sanders theory. Arch

Appl Mech 82:985–1002. https://doi.org/10.1007/s00419-011-0606-0
22. Qu Y, Long X, Wu S, Meng G (2013) A unified formulation for vibration analysis of composite laminated shells of revolution including shear deformation and rotary inertia. Compos Struct 98:169–191. https://doi.org/10.1016/j.compstruct.2012.11.001
23. Singh VK, Panda SK (2014) Nonlinear free vibration analysis of single/doubly curved composite shallow shell panels. Thin Walled Struct 85:341–349. https://doi.org/10.1016/j.tws.2014.09.003
24. Li H, Pang F, Miao X, Gao S, Liu F (2019) A semi analytical method for free vibration analysis of composite laminated cylindrical and spherical shells with complex boundary conditions. Thin Walled Struct 136:200–220. https://doi.org/10.1016/j.tws.2018.12.009
25. Sahoo SS, Panda SK, Mahapatra TR (2016) Static, free vibration and transient response of laminated composite curved shallow panel—an experimental approach. Eur J Mech A Solids 59:95–113. https://doi.org/10.1016/j.euromechsol.2016.03.014
26. Mahapatra TR, Panda SK (2016) Nonlinear free vibration analysis of laminated composite spherical shell panel under elevated hygrothermal environment: a micromechanical approach. Aerosp Sci Technol 49:276–288. https://doi.org/10.1016/j.ast.2015.12.018
27. Tornabene F, Fantuzzi N, Bacciocchi M, Neves AMA, Ferreira AJM (2016) MLSDQ based on RBFs for the free vibrations of laminated composite doubly-curved shells. Compos B Eng 99:30–47. https://doi.org/10.1016/j.compositesb.2016.05.049
28. Li H, Pang F, Wang X, Du Y, Chen H (2018) Free vibration analysis for composite laminated doubly-curved shells of revolution by a semi analytical method. Compos Struct 201:86–111. https://doi.org/10.1016/j.compstruct.2018.05.143
29. Pang F, Li H, Wang X, Miao X, Li S (2018) A semi analytical method for the free vibration of doubly-curved shells of revolution. Comput Math Appl 75–9:3249–3268. https://doi.org/10.1016/j.tws.2018.03.026
30. Alwar RS, Narasimhan MC (1990) Application of Chebyshev polynomials to the analysis of laminated axisymmetric spherical shells. Compos Struct 15:215–237
31. Lal A, Singh BN, Anand S (2011) Nonlinear bending response of laminated composite spherical shell panel with system randomness subjected to hygro-thermo-mechanical loading. Int J Mech Sci 53:855–866. https://doi.org/10.1016/j.ijmecsci.2011.07.008
32. Ferreira AJM, Carrera E, Cinefra M, Roque CMC (2011) Analysis of laminated doubly-curved shells by a layerwise theory and radial basis functions collocation, accounting for through-the-thickness deformations. Comput Mech 48:13–25. https://doi.org/10.1007/s00466-011-0579-4
33. Mahapatra TR, Panda SK, Kar VR (2016) Geometrically nonlinear flexural analysis of hygro-thermo-elastic laminated composite doubly curved shell panel. Int J Mech Mater Des 12:153–171. https://doi.org/10.1007/s10999-015-9299-9
34. Tornabene F, Brischetto S (2018) 3D capability of refined GDQ models for the bending analysis of composite and sandwich plates, spherical and doubly-curved shells. Thin Walled Struct 129:94–124. https://doi.org/10.1016/j.tws.2018.03.021
35. Katariya PV, Hirwani CK, Panda SK (2019) Geometrically nonlinear deflection and stress analysis of skew sandwich shell panel using higher-order theory. Eng Comput 35:467–485. https://doi.org/10.1007/s00366-018-0609-3
36. Katariya PV, Panda SK (2019) Numerical evaluation of transient deflection and frequency responses of sandwich shell structure using higher order theory and different mechanical loadings. Eng Comput 35:1009–1026. https://doi.org/10.1007/s00366-018-0646-y
37. Hirwani CK, Panda SK (2019) Nonlinear transient analysis of delaminated curved composite structure under blast/pulse load. Eng Comput 1:1–14. https://doi.org/10.1007/s00366-019-00757-6
38. Sayyad S, Ghugal YM (2019) Static and free vibration analysis of laminated composite and sandwich spherical shells using a generalized higher-order shell theory. Compos Struct 129:129–146. https://doi.org/10.1016/j.compstruct.2019.03.054
39. Evkin Y (2019) Composite spherical shells at large deflections. Asymptotic analysis and applications. Compos Struct. https://doi.org/10.1016/j.compstruct.2019.111577
40. Reddy JN (2003) Mechanics of laminated composites plates and shells. CRC Press, New York
41. Sanders JL (1959) An improved first-approximation theory for thin shells. NASA TR-24
42. Shin DK (1997) Large amplitude free vibration behavior of doubly curved shallow open shells with simply-supported edges. Comput Struct 62–1:35–49. https://doi.org/10.1016/S0045-7949(96)00215-5
43. Reddy JN (2006) Theory and analysis of elastic plates and shells, 2nd edn. CRC Press, New York
44. Hoppmann WH, Baronet CN (1963) A study of the vibrations of shallow spherical shells. J Appl Mech 30:329–334. https://doi.org/10.1115/1.3636557